SICE Annual Conference 2011
September 13-18, 2011, Waseda University, Tokyo, Japan

Path-Following Control of a Flexible-Base Manipulator Considering Dynamic Singularities and External Force

Naoyuki Hara[1], Daisuke Sato[2] and Yoshikazu Kanamiya[2]

Department of Mechanical Systems Engineering, Graduate School of Engineering, Tokyo City University, Japan
(Tel: +81-3-5707-0104 (3944); E-mail: [1]hara@rls.mse.tcu.ac.jp, [2]{sato, nenchev}@tcu.ac.jp)

Abstract: Dynamic singularities of a flexible-base manipulator cause a significant problem from viewpoint of control. This problem occurs when we control both the end-effector of the manipulator and the vibration of the flexible base simultaneously. In this paper, we propose a path-following control method with vibration suppression in the presence of dynamic singularities for a planar flexible-base three-link redundant manipulator model. Also, an external force can be dealt with using this control method. Results from several numerical simulations demonstrate the capability of the new control method.

Keywords: Flexible-base manipulator, Vibration suppression, Path-following control, Reactionless motion, Dynamic singularity

1. INTRODUCTION

Flexible-base manipulators represent a challenge from the control point of view. The reason is the dynamic coupling between the motion of the manipulator and that of the flexible base. The reaction force generated by the manipulator motion disturbs the base and induces vibrations. Moreover, the vibration adversely affects the accuracy of the end-effector positioning. Numerous studies on the problem exist already. Some deal with pure vibration suppression (VS) via inertial damping [1]. Others propose command generation for minimizing base disturbance [2]. In our previous study, we have introduced an approach aiming at base disturbance avoidance, based on reactionless motion (RLM) generation and control [3]. The approach employs the Reaction Null-Space (RNS) concept developed initially for free-floating space robots [4]. The main point was to take advantage of the dynamic coupling between manipulator and base. Unfortunately, the problem of dynamic singularities occurs when making use of the coupling.

Conventional singularity avoidance is not applicable in the case of dynamic singularities located within the workspace. In contrast to kinematic singularities, the loci of dynamic singularities change with the variation of the arm configuration thus rendering path planning for singularity avoidance a very difficult problem [5][6]. We have developed control methods for a planar flexible-base three-DOF redundant manipulator tracking a given end-tip path in the presence of dynamic singularities, as shown in Fig. 1. In [5], a RLM control method based on the RNS concept that achieves end-tip tracking control without any base vibrations was proposed. However, dynamic singularities due to the RLM constraint restrict the workspace of the manipulator. To alleviate this problem, in [6] we relaxed the RLM constraint by employing pseudoinverse-based end-tip path tracking control and VS control, making thereby use of the manipulator kinematic redundancy. Unfortunately, we have faced the problem of base disturbance generated by manipulator motion at dynamic singularities of VS. Fig. 1 (a) displays a dynamic singular configuration with regard to RLM and VS.

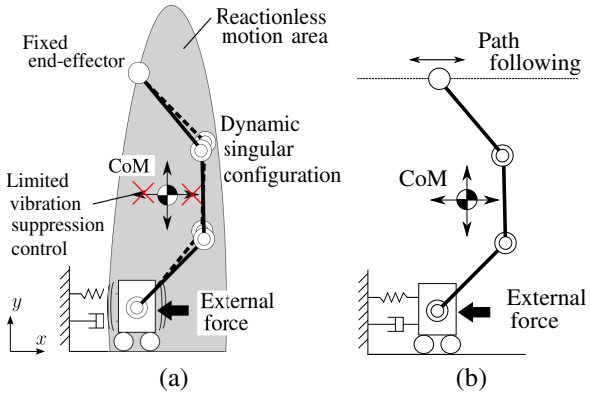

Fig. 1 Model of a planar flexible-base three-DOF redundant manipulator. (a) Example of a dynamically singular configuration. The manipulator workspace is restricted and the VS control is limited. (b) Path-following VS control method for resolving the problem of dynamic singularities.

Furthermore, we have proposed two switching control strategies for minimizing base disturbance in the vicinity of dynamic singularities. Specifically, through switching off VS in the vicinity [7] or switching from VS to momentum conservation (and vice versa) [8] we could achieve reactionless stable tracking control, based on proper definition of dynamics singularities. These switching control strategies show a good performance but the setting of control gains and proper thresholds for the definition of dynamic singularities is not as straightforward. Also, in these previous studies, we did not consider the presence of an external force.

The goal of the present study is to introduce a control method which can realize both end-tip path following and base VS considering dynamic singularities and the presence of an external force in the same time. In order to solve this problem, we will employ a path-following

method, such that end-tip position control along the path-following direction is relaxed. This is a technique similar to time scaling of the end-tip trajectory, known from previous studies [9], [10]. The idea is illustrated in Fig. 1 (b). It will be shown that with path-following control it is possible to address the problem of dynamic singularities, without the need of switching control in the neighborhood of dynamics singularities. Also, it will be shown that path-following control is helpful in handling external and/or imposed forces. Moreover, it will be shown that the combination of path-following VS and RLM control is helpful in designing a gross motion strategy for the flexible-base manipulator. We call this motion strategy *gross path-following VS motion strategy*.

2. BACKGROUND AND NOTATIONS

2.1 Equation of motion

The equation of motion of a flexible-base manipulator can be written in the following form [3]:

$$\begin{bmatrix} \boldsymbol{H}_b & \boldsymbol{H}_{bm} \\ \boldsymbol{H}_{bm}^T & \boldsymbol{H}_m \end{bmatrix} \begin{bmatrix} \dot{\mathcal{V}}_b \\ \ddot{\boldsymbol{q}} \end{bmatrix} + \begin{bmatrix} \mathcal{C}_b \\ \boldsymbol{c}_m \end{bmatrix} + \begin{bmatrix} \boldsymbol{D}_b \mathcal{V}_b \\ \boldsymbol{D}_m \dot{\boldsymbol{q}} \end{bmatrix} + \begin{bmatrix} \boldsymbol{K}_b \Delta\mathcal{X}_b \\ \boldsymbol{0} \end{bmatrix} = \begin{bmatrix} \mathcal{F}_{ext} \\ \boldsymbol{\tau} \end{bmatrix}, \tag{1}$$

where subscripts $(\circ)_m$ and $(\circ)_b$ mean manipulator and base, respectively. Caligraphic characters denote spatial vector quantities, e.g. the spatial (position/orientation) deflection of the base from its equilibrium $\Delta\mathcal{X}_b \in \Re^k$, the spatial velocity $\mathcal{V}_b \in \Re^k$ and the external spatial force $\mathcal{F}_{ext} \in \Re^k$ acting on the base. Henceforth, the spatial force will be referred to as force in short. $\boldsymbol{q} \in \Re^n$ stands for the generalized coordinates of the manipulator, $\boldsymbol{H}_b$, $\boldsymbol{D}_b$, and $\boldsymbol{K}_b \in \Re^{k\times k}$ denote base inertia, viscous damping and stiffness, respectively. $\boldsymbol{H}_m(\boldsymbol{q}) \in \Re^{n\times n}$ is the inertia matrix of the manipulator, $\boldsymbol{D}_m$ stands for joint viscous damping. Matrix $\boldsymbol{H}_{bm}(\Delta\mathcal{X}_b, \boldsymbol{q}) \in \Re^{k\times n}$ denotes the so-called inertia coupling matrix. $\mathcal{C}_b(\Delta\mathcal{X}_b, \boldsymbol{q}, \mathcal{V}_b, \dot{\boldsymbol{q}})$ and $\boldsymbol{c}_m(\Delta\mathcal{X}_b, \boldsymbol{q}, \mathcal{V}_b, \dot{\boldsymbol{q}})$ are velocity-dependent nonlinear terms, and $\boldsymbol{\tau} \in \Re^n$ is joint torque. No external force is acting on the manipulator.

2.2 Dual task formulation and dynamic singularities

We aim to simultaneously control both the end-tip motion and the base reaction. Let us consider first the motion of the flexible base. The base dynamics, derived from the equation of motion (1), can be written as:

$$\boldsymbol{H}_b \dot{\mathcal{V}}_b + \boldsymbol{D}_b \mathcal{V}_b + \boldsymbol{K}_b \Delta\mathcal{X}_b = \mathcal{F}_b + \mathcal{F}_{ext}, \tag{2}$$

where $\mathcal{F}_b \in \Re^k$ is defined as the *base reaction force* appearing in response to the force imposed on the base by manipulator motion:

$$\mathcal{F}_m = -\mathcal{F}_b = \boldsymbol{H}_{bm}\ddot{\boldsymbol{q}} + \mathcal{C}_b. \tag{3}$$

$\mathcal{F}_m$ will be henceforth referred to as the *imposed force*. We resolve the above equation as:

$$\ddot{\boldsymbol{q}} = \boldsymbol{H}_{bm}^{+}(\mathcal{F}_m - \mathcal{C}_b) + \boldsymbol{n}_{H_{bm}}, \tag{4}$$

where $(\circ)^+$ denotes the pseudoinverse, and $\boldsymbol{n}_{H_{bm}} \in \Re^n$ is a suitably chosen vector from the kernel of the inertia coupling matrix. The kernel is referred to as the *Reaction Null Space* [3]. We used this notation for VS, injecting thereby additional (inertial) damping into the base dynamics via the relation $\mathcal{F}_m^{ref} = \boldsymbol{G}_b \mathcal{V}_b$, $\boldsymbol{G}_b$ denoting a positive definite matrix for spatial damping. Thus, we obtain the following closed-loop system:

$$\boldsymbol{H}_b \dot{\mathcal{V}}_b + (\boldsymbol{D}_b + \boldsymbol{G}_b)\,\mathcal{V}_b + \boldsymbol{K}_b \Delta\mathcal{X}_b = \mathcal{F}_{ext}. \tag{5}$$

Thus, any base deflection due to $\mathcal{F}_{ext}$ can be suppressed.

Next, we focus on end-tip path tracking. Denote by $\mathcal{V}_e = \begin{bmatrix} \boldsymbol{v}_e^T & \boldsymbol{\omega}_e^T \end{bmatrix}^T \in \Re^m$ the end-tip spatial velocity. Its rate can be written as:

$$\dot{\mathcal{V}}_e = \boldsymbol{J}_e \ddot{\boldsymbol{q}} + \dot{\boldsymbol{J}}_e \dot{\boldsymbol{q}} + \dot{\mathcal{V}}_b, \tag{6}$$

where $\boldsymbol{J}_e(\boldsymbol{q}) \in \Re^{m\times n}$ is the end-tip Jacobian. The conventional PD path-tracking controller can be embedded by a proper choice of a reference end-tip acceleration $\dot{\mathcal{V}}_e^{ref}$.

Combining the imposed base motion constraint (3) with the above end-tip acceleration constraint, we obtain:

$$\begin{bmatrix} \dot{\mathcal{V}}_e^{ref} \\ \mathcal{F}_m^{ref} \end{bmatrix} = \boldsymbol{A}\ddot{\boldsymbol{q}} + \begin{bmatrix} \dot{\boldsymbol{J}}_e \dot{\boldsymbol{q}} \\ \mathcal{C}_b \end{bmatrix} + \begin{bmatrix} \dot{\mathcal{V}}_b \\ \boldsymbol{0} \end{bmatrix}, \tag{7}$$

where $\boldsymbol{A} = \begin{bmatrix} \boldsymbol{J}_e^T & \boldsymbol{H}_{bm}^T \end{bmatrix}^T \in \Re^{(m+k)\times n}$. A reference joint acceleration can be then obtained as:

$$\ddot{\boldsymbol{q}}^{ref} = \boldsymbol{A}^{+}\left(\begin{bmatrix} \dot{\mathcal{V}}_e^{ref} \\ \mathcal{F}_m^{ref} \end{bmatrix} - \begin{bmatrix} \dot{\boldsymbol{J}}_e \dot{\boldsymbol{q}} \\ \mathcal{C}_b \end{bmatrix} - \begin{bmatrix} \dot{\mathcal{V}}_b \\ \boldsymbol{0} \end{bmatrix} \right) + \boldsymbol{n}_A, \tag{8}$$

where $\boldsymbol{n}_A \in \Re^n$ denotes a suitably chosen vector from the kernel of $\boldsymbol{A}$. Note, the kernel is null when there are no redundant DOFs, namely $m + k = n$.

It would be straightforward to implement the above reference joint acceleration into a computed-torque controller. However, in the neighborhood of singularities of $\boldsymbol{A}$, the performance will inevitably degrade and the system may destabilize. These singularities include the subset of kinematic singularities where the rank of the Jacobian $\boldsymbol{J}_e$ degrades. Note that while kinematic singularities are static ones, the rest are of dynamic nature, located within the workspace. The loci of these singularities change continuously as a function of the manipulator configuration. We will refer to these latter singularities as *dynamic singularities*.

We attempted to tackle the singularity problem by resolving the dual-task control problem within a framework of task prioritization [11], involving in the same time the *Singularity-Consistent method* [12]. A higher priority for the inertial damping task leads to:

$$\ddot{\boldsymbol{q}}^{ref} = \boldsymbol{H}_{bm}^{+}(\mathcal{F}_m^{ref} - \mathcal{C}_b) + \boldsymbol{N}_{H_{bm}}(\dot{\mathcal{V}}_e^{ref})\boldsymbol{\beta}, \tag{9}$$

where $\boldsymbol{N}_{H_{bm}}(\dot{\mathcal{V}}_e) \in \Re^{(n-m)\times k}$, $\boldsymbol{\beta} \in \Re^k$ denoting an arbitrary vector, stands for the null-space vector $\boldsymbol{n}_{H_{bm}}$ in Eq. (4). It has been shown in [12], that in order to tackle

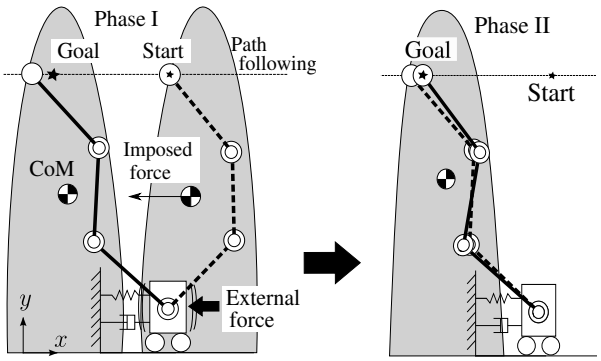

Fig. 2 Gross path-following VS motion strategy: (a) path-following VS control for coarse positioning; (b) RLM control for precise positioning.

the degraded function of the null-space vector at dynamic singularities, $\boldsymbol{\beta}$ should be constant. The stability of the system can be obtained via this technique, however, the workspace of the manipulator's end-tip is restricted.

A higher priority for the path-tracking task, on the other hand, leads to:

$$\ddot{\boldsymbol{q}}^{ref} = \boldsymbol{J}_e^{+}\left(\dot{\mathcal{V}}_e^{ref} - \dot{\boldsymbol{J}}_e\dot{\boldsymbol{q}} - \dot{\mathcal{V}}_b\right) + \boldsymbol{N}_{J_e}(\mathcal{F}_m^{ref})\boldsymbol{\beta}, \quad (10)$$

where $\boldsymbol{N}_{J_e}(\mathcal{F}_m^{ref})\boldsymbol{\beta}$ denotes a vector from the kernel of the manipulator Jacobian matrix, that depends upon the reference imposed force. Of course, dynamic singularities did not disappear, but it became possible to design a computed torque control law for avoiding destabilization during the path-following, by simply removing the null-space component in the last equation while crossing the singularities [7].

3. GROSS MOTION STRATEGY WITH PATH-FOLLOWING VIBRATION SUPPRESSION

The singularity problem can be related to the loss of DOF with regard to one of the tasks or both of them. To alleviate the problem, we employ a path-following control method that relaxes the constraint for strict time-dependent path tracking [8]. This means that a redundant DOF is made available because the end-tip DOF is decreased by one: $m-1$. The reference joint acceleration is derived from Eq. (8), wherein the dimension of the Jacobian and related quantities are properly adjusted. The null vector $\boldsymbol{n}_A$ is thereby not used because of the dynamic singularities.

The path-following VS control approach just introduced leads to the possibility of end-tip motion on a desired path with simultaneous vibration suppression within large portions of the workspace. The method cannot ensure, however, precise end-tip positioning at a specified point on the path. Therefore, we will combine the approach with a RLM controller that guarantees precise positioning without disturbing the base, albeit within a restricted workspace locally. The idea is illustrated in Fig. 2, where during Phase I a gross motion along the desired path is performed, resulting in coarse positioning in the vicinity of the desired position. Thereafter, reactionless fine positioning is done, within Phase II. It should be emphasized that the method allows us to also deal with external forces that can be easily accommodated with the help of the redundant DOF along the path. This will be demonstrated in the simulation study below.

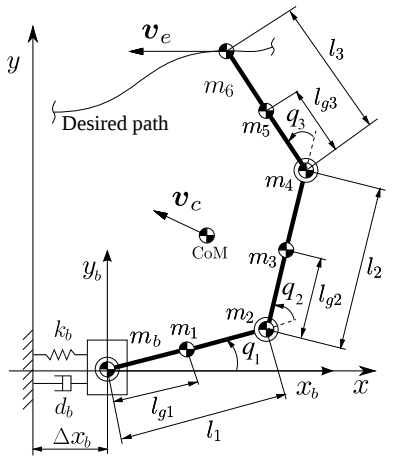

Fig. 3 Model of a planar three-link manipulator on a flexible base.

Table 1 The model parameters.

m_b	0.4 kg	l_1	0.1 m
m_1	0.025 kg	l_2	0.1 m
m_2	0.285 kg	l_3	0.1 m
m_3	0.025 kg	l_{g1}	0.05 m
m_4	0.285 kg	l_{g2}	0.05 m
m_5	0.025 kg	l_{g3}	0.05 m
m_6	0.095 kg	I_1	0.0135 kgm^2
k_b	191 N/m	I_2	0.0135 kgm^2
d_b	0.33 Ns/m	I_3	0.00307 kgm^2

Note: I_1, I_2 and I_3 are given w.r.t. the joint centers.

4. CASE STUDY

Let us consider a three-link planar manipulator on a flexible base deflecting in the x direction during the end-tip tracking as shown in Fig. 3. The model parameters of the three-link planar flexible-base manipulator are given in Table 1. The equation of motion can be arranged as:

$$\begin{bmatrix} h_b & \boldsymbol{h}_{bm} \\ \boldsymbol{h}_{bm}^T & \boldsymbol{H}_m \end{bmatrix}\begin{bmatrix} \dot{v}_b \\ \ddot{\boldsymbol{q}} \end{bmatrix} + \begin{bmatrix} c_b \\ \boldsymbol{c}_m \end{bmatrix} + \begin{bmatrix} d_b v_b \\ \boldsymbol{D}_m\dot{\boldsymbol{q}} \end{bmatrix} + \begin{bmatrix} k_b\Delta x_b \\ \boldsymbol{0} \end{bmatrix} = \begin{bmatrix} f_{ext} \\ \boldsymbol{\tau} \end{bmatrix}, \quad (11)$$

where $\boldsymbol{h}_{bm} \in \Re^{1\times 3}$ means the inertia coupling row-vector, respectively. v_b and Δx_b denote the base velocity and defection in the x direction, respectively. d_b and k_b describe the viscous damping and stiffness in the x direction, respectively. Since the system is planar, we will change henceforth the notation: $\mathcal{X} \to \boldsymbol{x}$, $\mathcal{V} \to \boldsymbol{v}$, $\mathcal{L} \to l$, $\mathcal{F} \to f$.

The driving torque needed to realize such a motion strategy is obtained from (11) as:

$$\boldsymbol{\tau}^{ref} = \boldsymbol{H}_m\ddot{\boldsymbol{q}}^{ref} + \boldsymbol{h}_{bm}^T\dot{v}_{bx} + \boldsymbol{D}_m\dot{\boldsymbol{q}} + \boldsymbol{c}_m. \quad (12)$$

We will perform a comparative performance analysis between three controllers: the pseudoinverse VS con-

troller, the reactionless VS controller and the newly introduced path-following VS controller.

According to Eqs. 9 and (10), pseudoinverse VS controller and reactionless VS controller can be derived as:

$$\ddot{\boldsymbol{q}}^{ref}_{\mathrm{rlvs}} = \boldsymbol{h}^{+}_{bm}(f^{ref}_{m} - c_b) + \beta \boldsymbol{n}_{h_{bm}}(\dot{\boldsymbol{v}}^{ref}_{e}), \tag{13}$$

$$\ddot{\boldsymbol{q}}^{ref}_{\mathrm{pivs}} = \boldsymbol{J}^{+}_{e}(\dot{\boldsymbol{v}}^{ref}_{e} - \dot{\boldsymbol{J}}_{e}\dot{\boldsymbol{q}} - \dot{\boldsymbol{v}}_b) + \beta \boldsymbol{n}_{J_e}(f^{ref}_{m}), \tag{14}$$

$$f^{ref}_{m} = f^{des}_{m} + g_b(v^{des}_{bx} - v_{bx}),$$

$$\dot{\boldsymbol{v}}^{ref}_{e} = \dot{\boldsymbol{v}}^{des}_{e} + \boldsymbol{K}_v(\boldsymbol{v}^{des}_{e} - \boldsymbol{v}_e) + \boldsymbol{K}_p(\boldsymbol{x}^{des}_{e} - \boldsymbol{x}_e),$$

respectively[1], where β and g_b are arbitrary scalars, $\boldsymbol{K}_v$ and $\boldsymbol{K}_p$ denote feedback gain matrices, $\boldsymbol{v}_b = [v_{bx}\ 0]^T$ stands for the base velocity vector and $\boldsymbol{x}_e = [x_{ex}\ x_{ey}]^T$ denotes the end-tip position. Note that the two null vectors $\boldsymbol{n}_{h_{bm}}$ and $\boldsymbol{n}_{J_e}$ impose a secondary task constraint and lead to dynamic singularities, such that $\det \boldsymbol{A} = \det \begin{bmatrix} \boldsymbol{J}^T_e & \boldsymbol{h}^T_{bm} \end{bmatrix}^T = 0$. To alleviate the problem, we will make use of the Singularity-Consistent approach [12] wherein the arbitrary scalar $\beta = |1/\det \boldsymbol{A}|$ outside the vicinity of a singularity, and is restricted to a constant value within the vicinity.

Next, we consider the path-following VS control method. For our planar example, the system rank decreases by one at a dynamic singularity. Hence, only two constraints can be ensured with the three-DOF manipulator. For simplicity, we will assume that the desired path is a straight line along the x coordinate. Therefore, the two constraints to be constantly enforced are VS along x and precise path-following along y. The reference joint acceleration[2] is:

$$\ddot{\boldsymbol{q}}^{ref}_{\mathrm{pfvs}} = \boldsymbol{B}^{+} \left(\begin{bmatrix} \dot{v}^{ref}_{ey} \\ f^{ref}_{m} \end{bmatrix} - \begin{bmatrix} \dot{\boldsymbol{J}}_{ey}\dot{\boldsymbol{q}} \\ c_b \end{bmatrix} \right), \tag{15}$$

$$\dot{v}^{ref}_{ey} = \dot{v}^{des}_{ey} + k_v(v^{des}_{ey} - v_{ey}) + k_p(x^{des}_{ey} - x_{ey}),$$

where $\boldsymbol{B} = \begin{bmatrix} \boldsymbol{J}^T_{ey} & \boldsymbol{h}^T_{bm} \end{bmatrix}^T$, k_v and k_p stand for feedback gains and $\boldsymbol{J}_{ey}$ is the 1×3 Jacobian for the y coordinate. f^{ref}_{m} is used for VS control. Note that the force direction coincides with the direction of the end-tip path. Hence, we can employ f^{ref}_{m} to shift the end-tip position in x. With Eq. (15) we can achieve both VS control and end-tip path-following control in the x direction, as shown in Fig. 1 (b).

5. SIMULATION STUDY

5.1 Path-following VS control with comparison

Simulation results from the performance of the above mentioned controllers, e.g. Eqs. (13), (14) and (15), will be shown first. The common initial configuration is set to $\boldsymbol{q} = [45\ 45\ 45]^T$ deg. This is the same configuration as shown in Fig. 1 (a). Recall that this is a dynamically singular configuration. The system is at rest in the beginning. The vicinity of the singularity is defined via the maximum value of $|\beta|$ which is set to 1.0×10^4 for all simulations. At 1 s, the base is disturbed by an impulsive force of magnitude $f_{ext} = 3$ N, acting for 50 ms. The initial position of the end-tip is to be kept constant during the motion, via PD feedback. The reference force is $f^{ref}_{m} = g_b(v^{des}_{bx} - v_{bx})$ and $v^{des}_{bx} = 0$, i.e. this is the VS control component. The feedback gains are set as: $\boldsymbol{K}_v = \mathrm{diag}\begin{bmatrix} 3.0 & 3.0 \end{bmatrix} \times 10^2\ \mathrm{s}^{-1}$ and $\boldsymbol{K}_p = \mathrm{diag}\begin{bmatrix} 4.0 & 4.0 \end{bmatrix} \times 10^4\ \mathrm{s}^{-2}$. The joint viscous damping coefficients are set as $\boldsymbol{D}_m = \mathrm{diag}\begin{bmatrix} 0.05 & 0.05 & 0.05 \end{bmatrix}^{\mathrm{T}}\ \mathrm{Nms/rad}$, while the injected additional base viscous damping is $g_b = 20\ \mathrm{Ns/m}$.

The simulation data are shown in Figs. 4∼6. With regard to each figure, (a) shows plots of the joint angles. (b) shows the values of $\det \boldsymbol{A}$ and β. (c) shows the magnitude of base disturbance, f_{ext}, and the base deflection. (d) displays the end-tip position errors. Note that the bottom part of (b) in Fig. 6 indicates the value of $\det \boldsymbol{B}$. Note also that "ET" means "end-tip." From all simulations it can be seen that, until 1 s, the condition is stable. From (b) it is apparent that $\det \boldsymbol{A}$ is zero while β is $1.0 \times 10^4\ \mathrm{m}^2$ because of the singularity. Base disturbance is identical in all cases, as seen from (c).

First, we applied pseudoinverse VS control, Eq. (14). After the disturbance, the value of β starts switching between the maximum and minimum values. This leads to base vibrations, but the system can be stabilized after a while, as apparent from Figs. 4 (c) and (d), respectively.

In the second simulation, we used reactionless VS control, Eq. (13). From Fig. 5 it becomes apparent that the system cannot be stabilized after the base disturbance. The reason is the presence of the dynamic singularity, which renders VS impossible in this case.

In the third simulation, we examined path-following VS control, Eq. (15). As shown in the upper part of Fig. 6 (b), the value of $\det \boldsymbol{A}$ is close to zero. On the other hand, the bottom part of Fig. 6 (b) shows that $\det \boldsymbol{B}$ is not zero. Actually, it is sufficient to focus on $\det \boldsymbol{B}$ only. It is seen that the base vibration has been suppressed instantly (see Fig. 6 (c)). This comes at a price: as expected, the positioning accuracy along x was not guaranteed, as shown in Fig. 6 (d). On the other hand, in the y direction faithful tracking can be confirmed. We can conclude then that path-following VS control can be used to handle base disturbances in the vicinity of dynamic singularities successfully.

5.2 Gross path-following VS motion strategy

Simulation results from the gross motion strategy with path-following VS control will be introduced. The initial configuration is the same as in the previous simulations: $\boldsymbol{q} = [45\ 45\ 45]^T$ deg. The base disturbance impulse is also the same, with magnitude of $f_{ext} = 3$ N acting for 50 ms at $t = 1$ s. The desired final end-tip position is set to $[-0.1\ \ 0.0]$ m, relatively to the initial end-tip position.

We have to inject first some initial energy, such that the end-tip can move in the desired direction. For this purpose, the desired imposed force is set to $f^{des}_{m} = -0.25$ N, acting for 2 s from the start. As already noticed, under path-following VS control, we can achieve only coarse

[1] The subscripts $(\circ)_{\mathrm{pivs}}$ and $(\circ)_{\mathrm{rlvs}}$ mean pseudoinverse VS and reactionless VS, respectively.

[2] The subscript $(\circ)_{\mathrm{pfvs}}$ means path-following VS control.

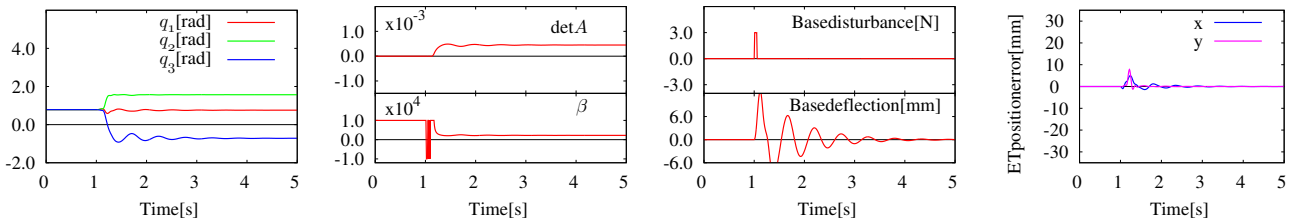

(a) (b) (c) (d)

Fig. 4 Simulation results with pseudoinverse VS control. The position errors and the base vibration due to the base disturbance cannot be suppressed instantly.

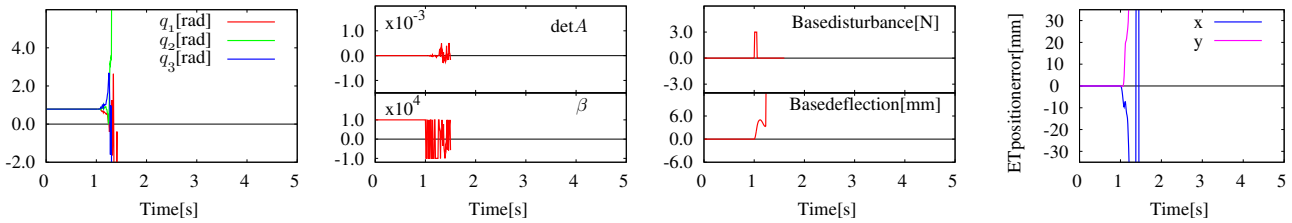

(a) (b) (c) (d)

Fig. 5 Simulation results with reactionless VS control. The positioning errors and the base vibration due to the base disturbance cannot be suppressed and then the system is destabilized.

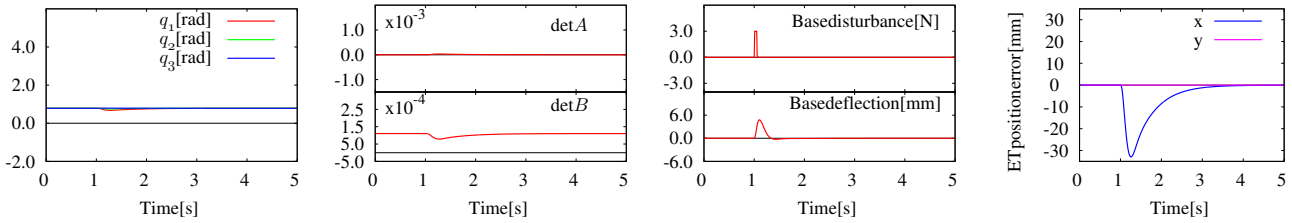

(a) (b) (c) (d)

Fig. 6 Simulation results with path-following VS control. Positioning error along x-axis can be tolerated. Base vibrations due to the base disturbance can be suppressed instantly.

positioning of the end-tip along x, during Phase I of the motion. The finial position will be accurately achieved by employing reactionless motion control, within Phase II of the motion.The distance from the inaccurate position at the end of Phase I to the accurate final position can be calculated easily on-line.

The injected additional base viscous damping is $g_b = 20\ \mathrm{Ns/m}$ with respect to Phase I. For Phase II, the feedback gains are set as: $k_v = \mathrm{diag}\begin{bmatrix}3.0 & 3.0\end{bmatrix} \times 10^2\ \mathrm{s}^{-1}$ and $k_p = \mathrm{diag}\begin{bmatrix}4.0 & 4.0\end{bmatrix} \times 10^4\ \mathrm{s}^{-2}$. The joint viscous damping coefficients are set as $\boldsymbol{D}_m = \mathrm{diag}\begin{bmatrix}0.05 & 0.05 & 0.05\end{bmatrix}^{\mathrm{T}}\ \mathrm{Nms/rad}$.

The results of the simulation are displayed in Fig. 7. (a) shows the RLM area at the initial configuration. (b) shows the trajectories of the end-tip and the CoM. (c) shows the joint angles. (d) displays the values of $\det \boldsymbol{A}$ and $\det \boldsymbol{B}$. (e) illustrates the desired imposed force and the end-tip position along x-axis. (f) displays base disturbance and base deflection. In Figs. 7 (a) and (b), the circle point and the asterisk point denote the initial and final positions, respectively. In Fig. 7 (e), the dashed line at -0.1 m stands for the final position. Phase I is from the beginning till 4 s, followed then by Phase II. It can be confirmed that the final position is out of the RLM area illustrated as dot map (see Fig. 7 (a)). The position of dots were calculated numerically by using the set of joint angles which can be obtained from the solutions of the CoM forward kinematics. To shift the RLM area, we inject energy into the system via the desired imposed force f_m^{des}, within Phase I. Since we don't aim to control the end-tip accurately, the end-tip position goes over the final position in the x direction, as seen from Fig. 7 (b). To obtain the accurate final position, reactionless VS control is employed in Phase II. This is possible, because the RLM area was shifted during Phase I.

From Fig. 7 (c), it is clearly seen how the joint angles evolve during the two phases. During Phase I, only the value of $\det \boldsymbol{B}$ matters because of the path-following VS control. Hence, as seen from Fig. 7 (d), the system is stable, despite $\det \boldsymbol{A}$ being almost zero. To ensure relocation of the RLM area, we apply the desired imposed force as illustrated in Fig. 7 (e). In addition, a base disturbance is applied at $t = 1$ s, as seen from Fig. 7 (f). Thereby, base deflection is induced, which, however can be suppressed instantly with the help of the VS control component. The end-tip reaches the boundary of the manipulator workspace at the end of Phase I, as shown in Fig. 7 (b).

With regard to Phase II, we employ reactionless VS control. That means, we cannot ignore the value of $\det \boldsymbol{A}$. It can be confirmed that the correct final end-tip position can be achieved, though, as shown in Fig. 7 (b)

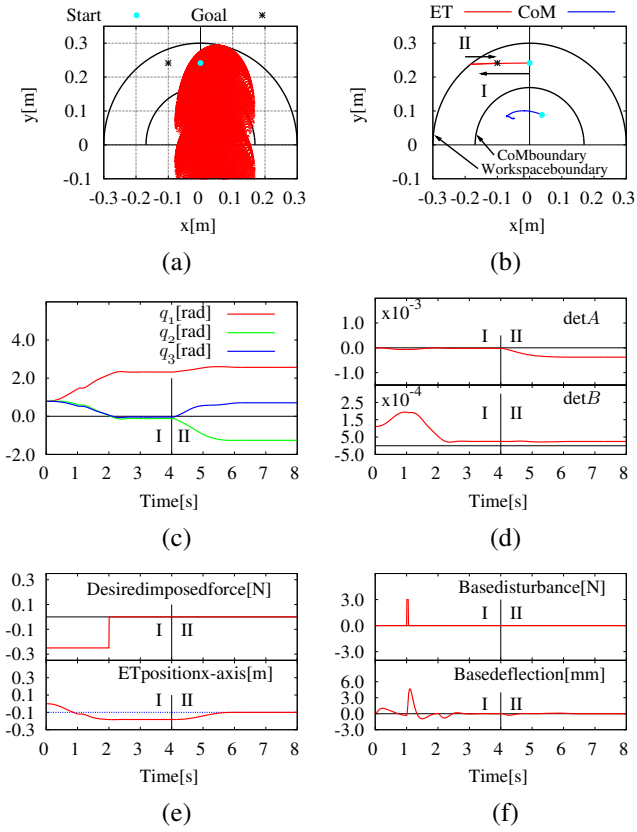

Fig. 7 Gross path-following VS motion strategy. Motion is initialized at a dynamic singularity. The goal position is outside the RLM area (shown in (a)). Phase I: Path-following VS control is employed, whereby a desired imposed force is applied from the beginning till $t = 2$ s to inject the energy needed to move the end-tip in the $-x$ direction along the desired path. Phase II: Reactionless VS motion is used to ensure the accurate final end-tip position.

and (e). The trajectory from the end of Phase I to the final position is generated via a fifth-order spline function. During Phase II, there is no desired imposed force and no external force, and also the base deflection is almost zero because of the reactionless VS control. The reason why the base deflection is not exactly zero is that there is the effect of the velocity-dependent term, c_b, as shown in Eq. (11). However the effect is quite small because of the relatively low-speed motion, as in this simulation.

6. CONCLUSION

We introduced a path-following VS control method to tackle problems related to the presence of dynamic singularities and base disturbances during end-tip path tracking with a flexible-base manipulator. The method was applied to a planar system comprising a single-DOF flexible-base and a three-DOF kinematically redundant manipulator mounted on it. The performance of the proposed control method was demonstrated by simulation experiments and compared with two other controllers developed in past studies.

Further on, the proposed path-following VS control method was combined with reactionless motion control into a gross motion strategy to achieve almost reactionless motion within a wide area of the workspace. Both controllers complement each other nicely, the former taking care of the dynamic singularities and accommodating base disturbances, and the latter ensuring precise positioning. From the experiments, it could be confirmed that the method has the potential to achieve the desired performance.

Still unsolved problems can be related to energy balance, e.g. the amount of injected energy needed to guarantee the shift of the RLM area in the vicinity of the goal point and to compensate energy dissipation during vibration suppression. Also, the calculation of the RLM area is still an open question. Model uncertainty and robustness issues should be addressed as well. These problems will be tackled in a future work.

REFERENCES

[1] S. H. Lee and W. J. Book, "Robot Vibration Control Using Inertial Damping Forces," in *Proceeding of 8th CISM–IFToMM Symposium RoManSy 8*, Cracow, Poland, 1990, pp. 252–259.

[2] D. W. Cannon *et. al*, "Experimental Study on Micro/Macro Manipulator Vibration Control," in *Proceeding of IEEE International Conference on Robotics and Automation*, Minneapolis, Minnesota, 1996, pp. 2549–2554.

[3] D. N. Nenchev *et. al*, "Reaction Null-Space Control of Flexible Structure Mounted Manipulator Systems," *IEEE Transaction on Robotics and Automation*, Vol. 15, No. 6, pp. 1011–1023, 1999.

[4] D. N. Nenchev, K. Yoshida and Y. Umetani, "Introduction of Redundant Arms for Manipulation in Space," in *IEEE International Workshop on Intelligent Robots and Systems*, Tokyo, Japan, 1988, pp. 679–684.

[5] T. Hishinuma and D. N. Nenchev, "Singularity-Consistent Vibration Suppression Control With a Redundant Manipulator Mounted on a Flexible Base," in *Proceeding of 2006 IEEE/RSJ International Conference on Intelligent Robots and Systems*, Beijing, China, 2006, pp. 3237–3242.

[6] Y. Fukazu *et. al*, "Pseudoinverse-Based Motion Control of a Redundant Manipulator on a Flexible Base With Vibration Suppression," *Journal of Robotics and Mechatoronics*, Vol. 20, No. 4, pp. 621–627, 2008.

[7] N. Hara *et. al*, "Singularity-Consistent Torque Control of a Redundant Flexible-Base Manipulator," in *Motion and Vibration Control*, Dordrecht, Netherlands, Springer Netherlands, pp. 103–112, 2008.

[8] N. Hara *et. al*, "Momentum Conserving Path Tracking Through Dynamic Singularities," in *Proceeding of the IEEE/RSJ International Conference on Intelligent Robots and Systems*, Taipei, Taiwan, 2010, pp. 5392–5397.

[9] J. M. Hollerbach, "Dynamic Scaling of Manipulator Trajectories," *Transaction of the ASME, Journal of Dynamic Systems, Measurement and Control*, Vol. 106, pp. 102–106, 1984.

[10] M. Sampei, and K. Furuta, "On Time Scaling for Nonlinear Systems: Application to Linearization," *IEEE Transaction on Automatic Control*, Vol. AC-31, No. 1, pp. 459–462, 1985.

[11] M. S. Konstantinov, M. D. Markov and D. N. Nenchev, "Kinematic Control of Redundant Manipulators," in *Proceeding of the 11th International Symposium on Industrial Robots*, Tokyo, Japan, 1981, pp. 561–568.

[12] D. N. Nenchev, Y. Tsumaki and M. Uchiyama, "Singularity-Consistent Parametrization of Robot Motion and Control," *International Journal of Robotics Research*, Vol. 19, No. 2, pp. 159–182, 2000.